SAND--88-2392C

DE89 013584

y OSTI

989

SOL-GEL PROCESSING OF CONTROLLED PORE FILMS

C. J. Brinker, G. C. Frye, A. J. Hurd, K. J. Ward, and C. S. Ashley

Sandia National Laboratories, Albuquerque, NM 87185-5800

Abstract

During sol-gel film formation via dipping, polymeric precursors are aggregated on the substrate surface by a process involving gravitational flow, drying, and continued condensation reactions. To understand film formation in situ, we use ellipsometric imaging and infrared spectroscopy. The structure and porosity of the deposited film are determined by SAXS, ellipsometry, and surface acoustic wave (SAW) methods. We find that weakly-branched silicate precursors deposited near the isoelectric point of silica result in dense films (volume percent porosity, $V_p < 5\%$) in which any pores present have radii < 0.2 nm, regardless of precursor size. More compact precursors result in films in which the porosity and refractive index are controlled by the size of the precursor species prior to deposition and the relative rates of condensation and evaporation during deposition. The porosity and refractive index of these films may be varied as follows: volume percent porosity ($0 \leq V_p \leq 56\%$); pore radius ($0 \leq r \leq 3.1$ nm); surface area ($1.2 \leq S \leq 263$ m^2/g); refractive index ($1.18 \leq n \leq 1.45$). For repulsive, monosized particulate precursors, higher coating rates promote ordering providing an additional means of pore size control.

1. Introduction

During sol-gel thin film formation via dipping or spinning, oligomeric or polymeric precursor species often described by mass or surface fractal dimensions, D or D_s † [1], are rapidly aggregated on the substrate surface

†: The mass fractal dimension, D, relates the mass of an object, M, to its radius r: $M \sim r^D$. The surface fractal dimension, D_s, varies from 2 for a smooth surface to 3 for a surface so convoluted that it fills space.

MASTER

DISTRIBUTION OF THIS DOCUMENT IS UNLIMITED

DISCLAIMER

This report was prepared as an account of work sponsored by an agency of the United States Government. Neither the United States Government nor any agency thereof, nor any of their employees, makes any warranty, express or implied, or assumes any legal liability or responsibility for the accuracy, completeness, or usefulness of any information, apparatus, product, or process disclosed, or represents that its use would not infringe privately owned rights. Reference herein to any specific commercial product, process, or service by trade name, trademark, manufacturer, or otherwise does not necessarily constitute or imply its endorsement, recommendation, or favoring by the United States Government or any agency thereof. The views and opinions of authors expressed herein do not necessarily state or reflect those of the United States Government or any agency thereof.

DISCLAIMER

Portions of this document may be illegible in electronic image products. Images are produced from the best available original document.

by gravitational or centrifugal draining accompanied by vigorous solvent evaporation and continued condensation reactions. Our previous research [2] has shown that the film porosity (calculated from the refractive index on the basis of the Lorentz-Lorenz relationship) depends on the compactness (D, D_s) and extent of branching of the precursors prior to deposition and the relative rates of condensation and evaporation during deposition. Precursor structure dictates steric constraints according to [3]:

$$M_{1,2} \propto R^{D_1 + D_2 - d} \qquad (1)$$

where $M_{1,2}$ is the probability of intersection of two mass fractal objects of size R and mass fractal (or Euclidian) dimensions, D_1 and D_2, placed independently of each other in the same region of space, and d is the dimension of space, 3. When D_1 and D_2 are ≤ 1.5, $M_{1,2}$ decreases indefinitely as the polymer size increases: the structures are mutually transparent and should interpenetrate as their concentration is increased, leading to dense films. de Gennes [4] envisioned such networks as "entangled worms". If D_1 and D_2 are greater than 1.5, the probability of intersection increases algebraically with R: the structures, though often porous, are "mutually opaque", similar to an assemblage of tumbleweeds.

The above discussion assumes that all intersections result in irreversible condensation reactions (sticking probability = 1) and that the precursor structures are completely rigid. In reality the structures are more or less compliant, since, e.g., the elastic modulii of fractal objects decrease with R [5]. Furthermore, the sticking probability is $<<1$ and is a sensitive function of pH as indicated by the pH-dependence of gel times in aqueous and alcoholic silicate solutions [6, 7]. These factors mitigate the criteria for mutual transparency, since few intersections result in

condensation, and the compliancy of the structures reduces the effectiveness of screening according to Eq. 1.

The relative rates of condensation and evaporation dictate chemical constraints. During film formation, a competition is established between evaporation and continuing condensation reactions. Evaporation tends to compact the film structure first by concentration and later by the capillary pressure exerted as the liquid-vapor interface recedes into the film interior. Condensation reactions at points of intersection inhibit interpenetration, according to the concepts of mutual opacity, and stiffen the structure, consequently increasing its resistance to compaction by the capillary pressure. For reacting systems, both increasing the condensation rate and reducing the evaporation rate allow more condensation reactions to occur during the brief time of film formation†, resulting in more porous films. Conversely, reducing the condensation rate and/or increasing the evaporation rate reduce the number of condensation reactions that occur during film formation leading to denser films. We will show, however, that for non-reacting systems of repulsive particles, increasing the drying time allows ordering to occur, leading to denser films.

This paper explores how precursor structure and deposition conditions influence the porosity of thin sol-gel films prepared by dipping. This study extends our previous work [2] by providing a measure of the pore size and surface area of the deposited films in addition to the pore volume. We show that the pore size can be precisely tailored, suggesting applications as materials for sensors, filtration, or separation processes.

---

†: The time of film formation is generally several seconds comprising aging, gelation, and drying that convert the wet layer at the reservoir surface to a completely dry film normally a few cm above the reservoir surface.

2. Experimental

Three classes of precursors were prepared: (1) rather weakly-branched silicates (composition A2 in ref. 8) characterized by D = 1.9, deposited near pH 2; (2) more highly-branched, compact clusters (prepared according to ref. 9) characterized by D = 2.4, deposited between pH 3.5 and 1; and (3) dense colloidal particles (non-fractal) synthesized by variations of the Stöber process [10] and deposited above pH 10.

Films were deposited at room temperature on polished <100> single-crystal silicon (ellipsometry experiments); ST-cut crystalline quartz (SAW experiments); MYLAR or v-SiO_2 (SAXS experiments); or Au coated glass substrates (FTIR experiments). Subsequent measurements employed room temperature dried films or films heated to 400°C for 5 min. (Note: prior to SAW measurements films were reheated to 160°C for 2 h)

Prior to deposition the solutions were characterized by SAXS, quasi-elastic light scattering (QELS) or FTIR. Scattering data were analyzed in the Porod regime [11] to obtain structural information. Film structure was investigated in situ during deposition using imaging ellipsometry [12] or FTIR microscopy [13]. The structure of the deposited films was investigated by ellipsometry to obtain thickness and refractive index data and by performing N_2 adsorption experiments using a SAW technique [14] to obtain surface area and pore size information.

3. Results and Discussion

3.1 Weakly-branched System

Our previous work [2] indicated that weakly-branched precursors deposited near the isoelectric point of silica (pH 1-2 [7]) yielded dense films with $n \geq 1.425$ (corresponding to <5% porosity based on the refractive index of v-SiO_2, viz. 1.458) regardless of the precursor size, which was

varied by over one order of magnitude. Consistent with these results the corresponding N_2 adsorption isotherm (Figure 1a) is a Type II isotherm [15] indicating adsorption on a non-porous surface. Thus any porosity that exists has openings smaller than the kinetic radius of N_2 (~0.2 nm). The measured surface area, S = 0.95 cm^2/cm^2, corresponds approximately to the geometric area of the film surface, 1 cm^2/cm^2.

Several factors contribute to the high density of these films: 1) the brief deposition time combined with a low condensation rate allows little further condensation to occur during deposition; 2) the weakly-branched, compliant polymers are able to interpenetrate and rearrange themselves to progressively denser configurations in response to the evaporating solvent; 3) because the extent of condensation remains low, the compliant films are further compressed at the final stage of drying by the capillary pressure which can now be enormous (1-2 kbar [16]) due to the preceeding shrinkage that reduces the effective pore size to molecular dimensions. This collapse is illustrated by the refractive index profile of a drying film determined from imaging ellipsometry: Figure 2 shows a narrow region near the drying front where the index suddenly increases.

The importance of the brief time-scale of the film deposition process compared to the bulk gel process is illustrated in Fig. 1b, which shows the N_2 adsorption-desorption isotherm of a monolithic gel prepared from the identical silicate precursors used for the film (Fig. 1a). The monolithic sample, which was gelled and dried over a period of several months, becomes much more highly condensed (stiffer) at an earlier stage of the drying process. Therefore it shrinks less during the initial stage of drying where it is completely filled with liquid, causing the capillary pressure

during the final stage of shrinkage to be reduced due to the larger effective pore size. In addition the resistance to the capillary pressure is increased due to the increased stiffness. The result is a less dense, microporous gel as indicated by the large amount of adsorption at low N_2 pressures characteristic of a Type I isotherm [15]. This result contrasts dramatically with the dense films formed from the same precursors on a much shorter time scale.

3.2 Strongly-Branched System

The stongly branched system deposited at pH 3.4 exhibts a reciprocal relationship between precursor size and refractive index, i.e., films deposited from solutions containing progressively larger-sized polymeric precursors (obtained by aging at 50°C) exhibit progressively lower refractive indices (see Table 1). Since for mass fractals, density, ρ, decreases radially as

$$\rho \sim 1/r^{(3 - D)}, \qquad (2)$$

this behavior is consistent with an assemblage of mutually opaque mass fractal clusters: the porosity of an assemblage of clusters should increase with cluster size (assuming that the clusters do not completely collapse). The Porod plot of a film prepared from precursors aged for 14 days (Fig. 3) is composed of two limited power law regions corresponding to $D = 1.7$ and $D = 2.8$ separated by a transition region ($K^{-1} \sim 1.7$ to 1.3 nm). The corresponding pore size distribution obtained from the SAW desorption isotherm (inset Fig. 3) indicates that the transition occurs at about the mean pore radius, ~ 1.9 nm. The SAXS and pore size data suggest that the individuals clusters ($D = 2.4$) are compacted during deposition due to the capillary pressure, causing D to increase to 2.8 on length scales < 1.3 nm.

The D value of 1.7 is consistent with simulations of transport-limited cluster-cluster aggregation (Fig. 3). This suggests that on length scales greater than ~ 1.7 nm the compacted clusters are aggregated creating interconnected porosity with "throat" radii ~ 1.9 nm. We speculate that the aggregation process appears to be transport-limited rather than reaction-limited (D = 2.1), because the rapidly increasing viscosity "freezes-in" a non-equilibrium configuration.

Based on this aggregation model, it is expected that the pore size should increase with cluster size. Table 1 shows that the mean pore radius determined from the desorption isotherms by standard calculation procedures [17] increases from < 0.2 to > 3.1 nm with the duration of aging at 50°C prior to deposition. The isotherm obtained for the film prepared from unaged precursors is a Type II isotherm indicative of a non-porous film ($r < 0.2$ nm, the kinetic radius of N_2, and $S = 1.2$ cm^2/cm^2, approximately the geometric area of the film surface). This suggests that, due to the small effective pore size, the film is collapsed during the last stage of deposition by the high capillary pressure. Larger, opaque clusters presumably increase the effective pore size causing the capillary pressure to decrease, resulting in more porous films. For example, Fig. 4 shows the N_2 adsorption-desorption isotherm obtained from the 1-week-aged precursor. It is a Type IV isotherm characteristic of a mesoporous solid [15]. The surface area has increased to 220 m^2/g (Table 1), and the pore size distribution (inset Fig. 4) is narrow and centered at ~1.6 nm.

Table 1 clearly shows a correlation between pore volume (or refractive index) and pore size: pore volume increases (refractive index decreases) with pore size as a consequence of the fractal model described above. Unfortunately this does not allow the preparation of films with large

volumes of extremely small pores. However, since precursor aging times less than 3 days result in refractive indices that vary between 1.31 and 1.45, according to the above correlation, an advantage of this process should be the preparation of microporous films with pore radii ranging from 0.2 to 1.6 nm, sizes of interest for sensors and gas separations. SAW studies of these films are currently in progress.

As described above, a condition for mutual opacity of mass fractal objects is condensation reactions at points of intersection. Therefore a reduction in the condensation rate should reduce opacity, resulting in denser films. This hypothesis was tested by depositing 1-week-aged precursors at pH values ranging from about 3.2 to 1.2. In situ FTIR reflectance microscopy (Fig. 5) shows that at pH 3.2 condensation reactions, characterized by increased relative intensity and broadening of the Si-O assymetric stretching vibration centered at 1180 cm^{-1}, accompany film deposition. Fig. 6 shows that the refractive index increases as the pH is reduced below pH 3.2 by additions of 2M HCl immediately prior to deposition. Equivalent additions of H_2O cause no consistent changes in refractive index. This result suggests that HCl additions reduce the condensation rate facilitating interpenetration and contributing to compliancy†. As described above, both factors promote compaction of the film. By analogy to the correlation between refractive index and pore size shown in Table 1, changes in the relative rates of condensation and evaporation during deposition should provide an alternate method of pore size control utilizing a single solution aging condition.

---

†: A similar effect would be obtained if HCL promoted depolymerization; however the dissolution rate of silica is minimized in this pH range [6].

3.3 Particulate Films

Using opaque, monosized, particulate precursors, the porosity is controlled by the particle size and extent of aggregation or ordering. Our previous work [2] has shown that aggregation and deposition of silicate spheres at pH 7, where the silica condensation rate is maximized, results in films with porosities exceeding 65% compared to a minimum of 25% corresponding to FCC or hexagonal close packing. This high porosity is created in a manner similar to that described for the strongly-branched system in Section 3.2: consistent with the concept of mutual opacity (Eq. 1), aggregation results in fractal clusters (D = 2.1) that do not interpenetrate due to the large D and the high condensation rate. In addition, the capillary pressure is reduced, since the effective pore size is approximately the aggregate size. At comparable coating rates, deposition of the particles at pH 11 where they are mutually repulsive [6, 7] causes the porosity to decrease to about 42%. SAXS studies [2] indicate that under these conditions aggregation is avoided, presumably due to repulsive forces, and a liquid-like structure is frozen-in at the final stage of drying. Figure 7 shows that at high pH a further decrease in the pore volume (increase in the refractive index) occurs as the coating rate is increased. For example, increasing the coating rate from 2 to 30"/min (5 to 76.2 cm/min) causes the refractive index of the film prepared from 55 nm particles to increase from 1.2 to 1.34, corresponding to a reduction in V_p from 52 to 24%. For base concentrations exceeding 0.001 M, this trend of increasing refractive index with coating rate is observed for all silicate particles we have investigated (particle diameters $\approx$ 20-95 nm, see Fig. 7). By comparison the weakly-branched and strongly branched systems deposited at lower pH show a slight trend of decreasing refractive index

with coating rate (see, e.g., polymer sample in Fig. 7), since there is a greater time for condensation reactions to occur.

Our present interpretations of these trends of changing refractive index with coating rate are based on the relative rates of condensation and concentration (via solvent evaporation) and/or the possibility of shear-induced alignment. Since drying occurs exclusively from the film/vapor interface, which is independent of the film thickness, and higher coating rates produce thicker films, thick films take longer to dry thin films. Normally, when the condensation rate is finite, longer drying times allow additional crosslinking to occur, leading to more porous gels. This is well illustrated by the comparison of thin films and monoliths in Fig. 1 and explains the trend of decreasing refractive index with coating rate (polymer sample, Fig. 7). However if the particles are mutually repulsive (condensation rate = 0), longer drying times provide the necessary time for particle ordering leading to denser films. In addition, based on molecular dynamics calculations [18], it is expected that increased shear rates achieved by higher coating speeds will aid the ordering process. From the standpoint of pore size control, ordered packings of monosized particles should provide precise control of throat sizes defined by the interstice created by three touching spheres, providing a means of achieving large pores with narrow size distributions.

4. Summary

The porosity of sol-gel thin films prepared by dipping depends on the precursor structure, the relative rates of condensation and evaporation (or concentration) during deposition, and the coating rate.. Using three different classes of precursors, we have demonstrated that the porosity of

sol-gel thin films can be varied over wide ranges. Weakly branched precursors deposited under conditions where the condensation rate is low result in dense films with pore radii less than the kinetic radius of N_2. Strongly branched, compact precursors exhibit variable porosities (V_p = 0 to >50%, r = 0 to 3.0 nm, S = 1 - 245 m^2/g) that depend on the precursor size and the deposition conditions. Monosized particulate precursors appear to order when applied at high coating rates, providing a potential method for achieving rather large pore sizes with very narrow size distributions.

Acknowledgements

The authors acknowledge S.T Reed for assistance in film formation and deposition and A.J. Ricco and S.J. Martin for contributions to the SAW measurements

References

1. B. B. Mandelbrot, Fractals, Form, and Chance (Freeman, San Francisco, 1977).
2. C. J. Brinker, A. J. Hurd, and K. J. Ward in Ultrastructure Processing of Advanced Ceramics, Eds., J. D. Mackenzie and D. R. Ulrich (Wiley, NY, 1988) 223.
3. B. B. Mandelbrot, The Fractal Geometry of Nature, (Freeman, San Francisco, 1982).
4. P. G. deGennes, Physics Today, 36 (1983) 33-39.
5. T. A. Witten and M. E. Cates, Science, 232 (1986) 1607.
6. R. K. Iler, The Chemistry of Silica (Wiley, NY, 1979).

7. B. K. Coltrain, S. M. Melpolder, and J. M. Salva, this proceedings, p xxx.

8. C. J. Brinker, K. D. Keefer, D. W. Schaefer, R. A. Assink, B. D. Kay, C. S. Ashley, J. Non-Cryst. Solids, 63 (1984) 45.

9. C. S. Ashley and S. T. Reed, Sandia National Laboratories, Report SAND84-0662 (1984) (available from NTIS).

10. W. Stöber, A. Fink, and E. Bohn, J. Colloid Interface Sci., 26 (1968) 62.

11. G. Porod, Kolloid Z., 124 (1951) 83.

12. A. J. Hurd and C. J. Brinker, J. de Phys., 47 (1988) 1017.

13. K. J. Ward, unpublished

14. G. C. Frye, A. J. Ricco, S. J. Martin, and C. J. Brinker, in Better Ceramics Through Chemistry III, eds. C. J. Brinker, D. E. Clark, and D. R. Ulrich (Mat. Res. Soc., Pittsburgh, PA, 1988) p. 349.

15. S. J. Gregg and K. S. W. Sing, Adsorption, Surface Area and Porosity, (Academic Press, NY, 1982).

16. G. W. Scherer, this proceedings, p. XXX.

17. S. Lowell and J. E. Shields, Powder Surface Area and Porosity, (Chapman and Hall, NY, 1984).

18. J. H. Simmons, R. K. Mohr, and C. J. Montrose, J. Appl. Physics, 53 (1982) 4075.

DISCLAIMER

This report was prepared as an account of work sponsored by an agency of the United States Government. Neither the United States Government nor any agency thereof, nor any of their employees, makes any warranty, express or implied, or assumes any legal liability or responsibility for the accuracy, completeness, or usefulness of any information, apparatus, product, or process disclosed, or represents that its use would not infringe privately owned rights. Reference herein to any specific commercial product, process, or service by trade name, trademark, manufacturer, or otherwise does not necessarily constitute or imply its endorsement, recommendation, or favoring by the United States Government or any agency thereof. The views and opinions of authors expressed herein do not necessarily state or reflect those of the United States Government or any agency thereof.

Table Captions

1. Porosity versus aging conditions for the weakly-branched precursor aged at 50°C and pH 3.2 for the indicated times prior to deposition by dipping. *The 3 week sample was gelled and re-liquified ultrasonically prior to deposition.

Figure Captions

1. a) N_2 adsorption desorption isotherm obtained by the SAW technique for a film prepared from the weakly-branched precursor. b) Corresponding N_2 adsorption-desorption isotherm for a bulk, monolithic gel prepared from identical precursors as in Fig. 1a [13].
2. Index of refraction of a drying sol-gel film versus position on the substrate determined by imaging ellipsometry. The drying line is at approximately x = 0. The solid and dotted line at y = 1.401 indicates the refractive index of the dry film.
3. SAXS Porod plot of a film deposited from the strongly-branched system after 2 weeks of aging. Slopes corresponding to D = 2.8 and D = 1.7 indicate compaction on short length scales (<1.4 nm) and cluster-cluster aggregation on longer length scales. The cross-over occurs at approximately the mean pore size, viz. 1.9 nm.
4. Type IV N_2 adsorption-desorption isotherm obtained for a film prepared from the strongly-branched system after 1 week of aging. Inset: pore size distribution determined from the desorption branch.
5. FTIR reflection spectra obtained in situ at positions 15.7 mm above the coating bath and > 2cm above the coating bath (corresponding to a dried film).

6. Refractive index and pore volume for films prepared from the strongly-branched system after about 1 week of aging versus the deposition pH achieved by additions of 2 M HCl (aqueous). Squares denote equivalent additions of water.

7. Coating rate dependence of the refractive index for films prepared from a series of monosized particulate precusors (particle diameters = 20 to 95 nm) deposited at ~ pH 11 compared to the coating rate dependence of refractive index for films prepared from the strongly-branched system after 2 weeks of aging (denoted polymer).

Porosity versus Aging Conditions

Sample	Refractive Index	Porosity Ads. N_2	Median Pore Radius (nm)	Surface Area m^2/g
Unaged	1.45	0	< 0.2	1.2 - 1.9
3 Day	1.31	16	1.5	146
1 Week	1.25	24	1.6	220
2 Week	1.21	33	1.9	263
3 Week*	1.18	52	3.0	245

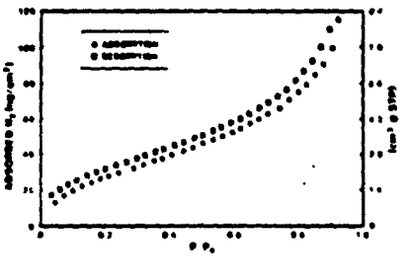

1a

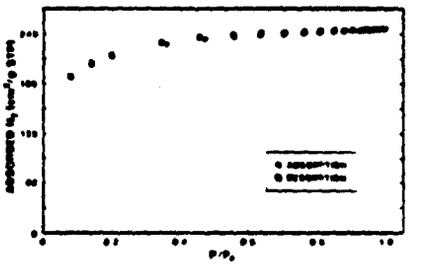

1b

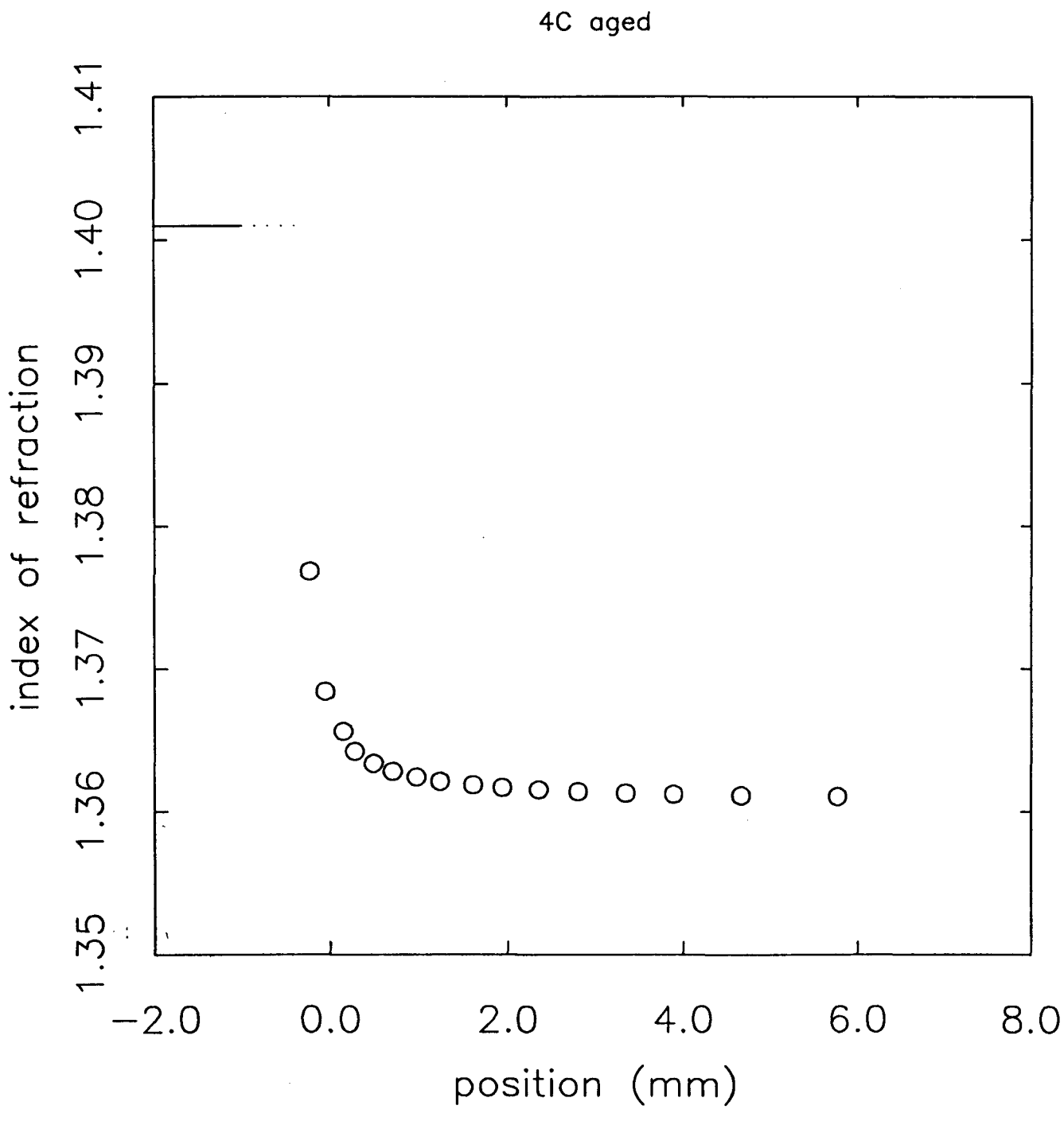
4C aged
index of refraction
1.35
1.36
1.37
1.38
1.39
1.40
1.41
−2.0
0.0
2.0
4.0
6.0
8.0
position (mm)

CLUSTER - CLUSTER - AGGREGATION

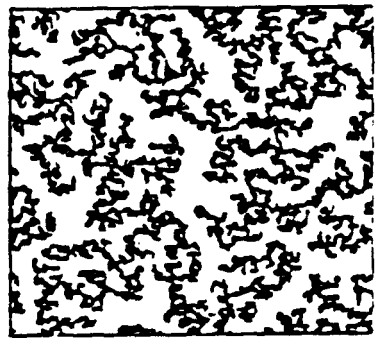

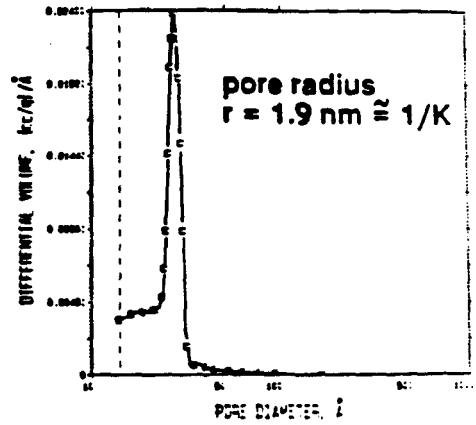

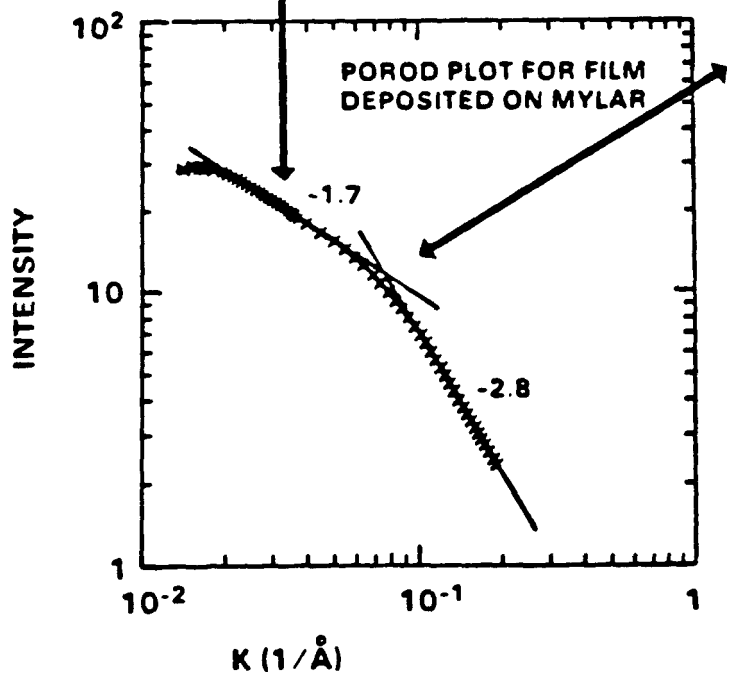

Porod plot for film deposited on MYLAR indicates either 1.4 nm pore sizes or compaction on short length scales < 1.4 nm, and cluster-cluster aggregation on long length scales

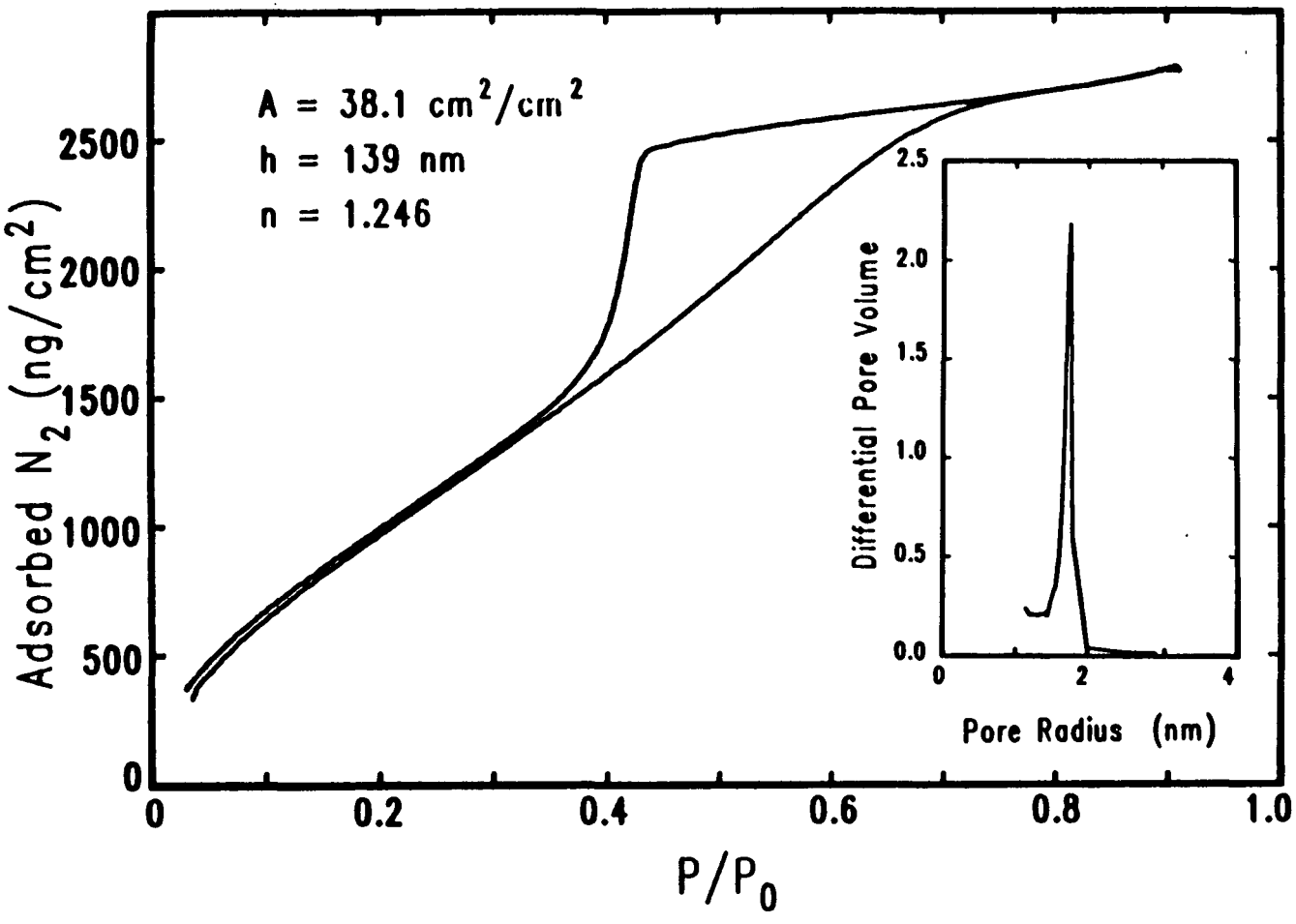
A = 38.1 cm²/cm²
h = 139 nm
n = 1.246
Adsorbed N2 (ng/cm²)
2500
2000
1500
1000
500
0
0
0.2
0.4
0.6
0.8
1.0
P/P0
Differential Pore Volume
2.5
2.0
1.5
1.0
0.5
0.0
0
2
4
Pore Radius (nm)

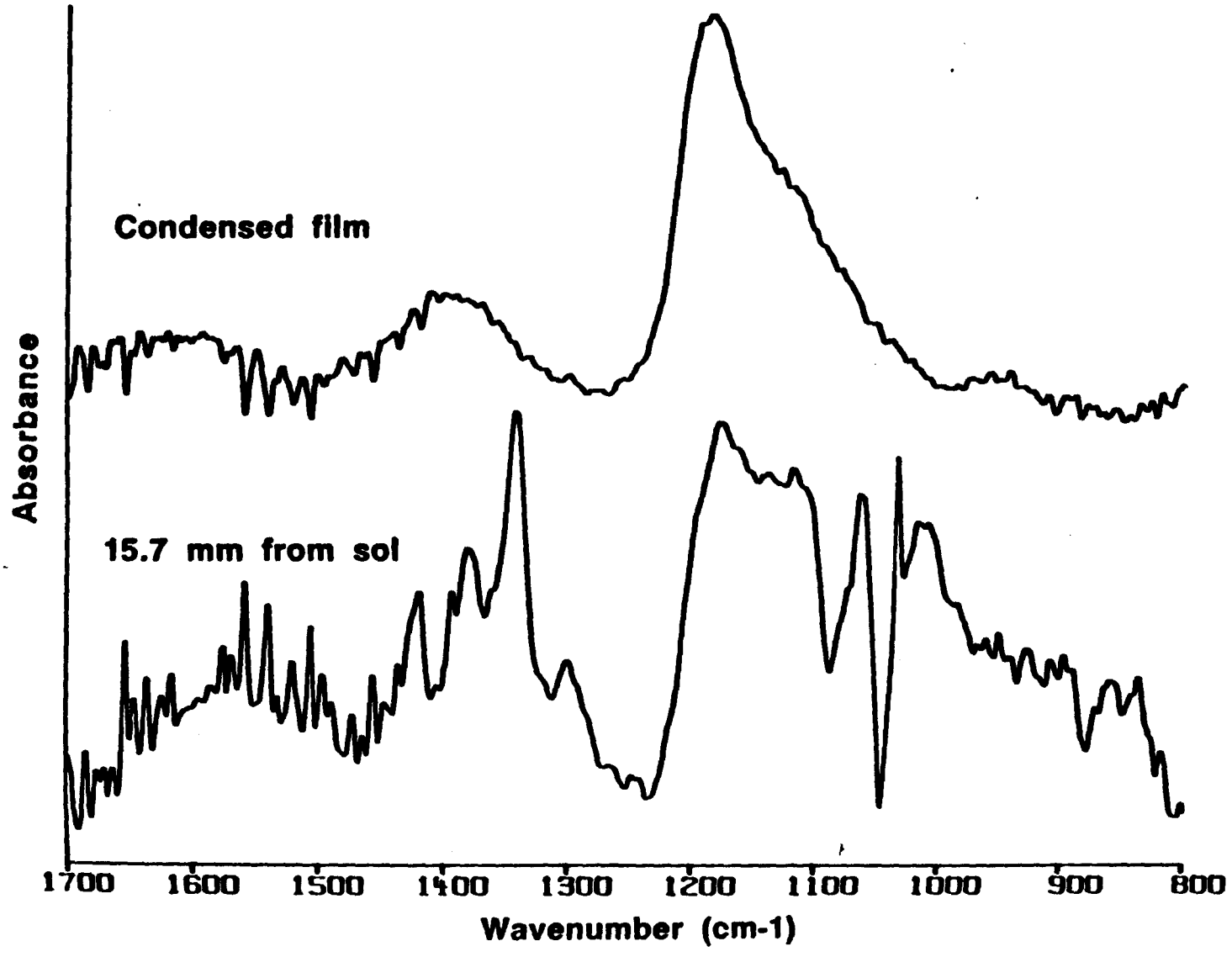
Condensed film
15.7 mm from sol
Absorbance
1700
1600
1500
1400
1300
1200
1100
1000
900
800
Wavenumber (cm-1)

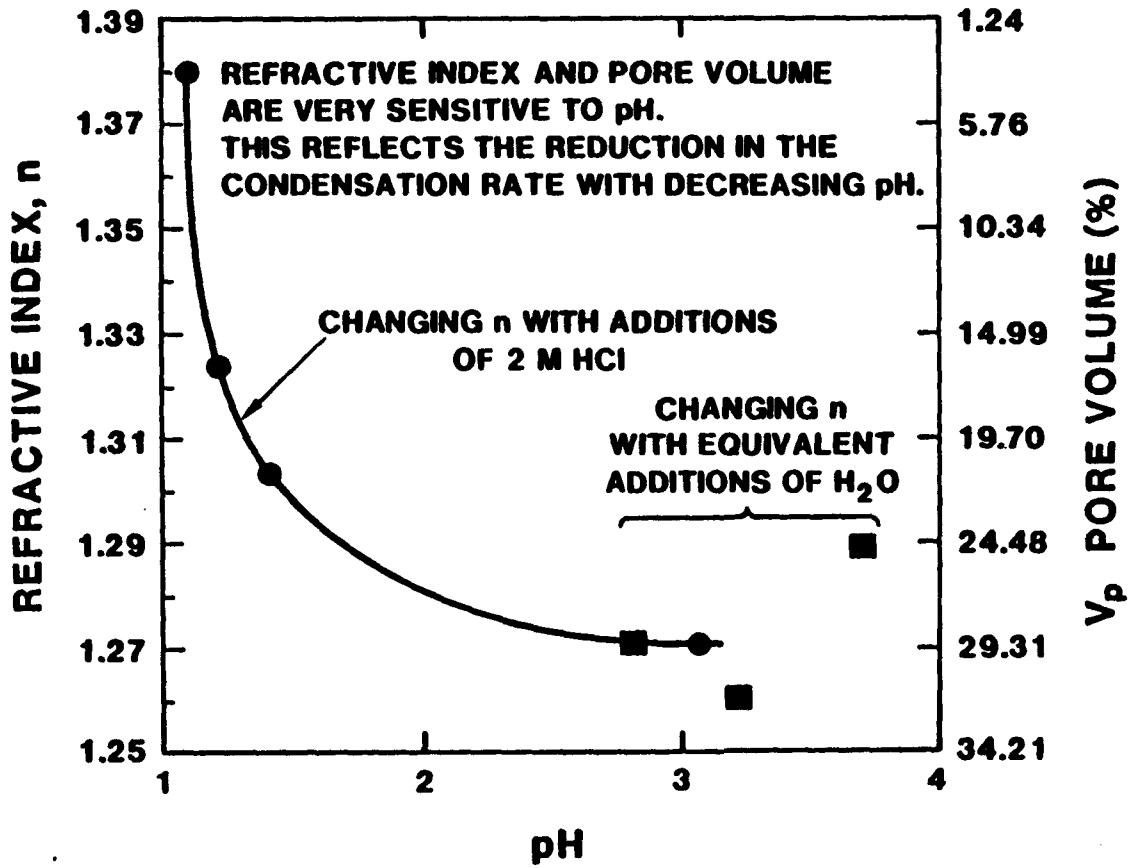
REFRACTIVE INDEX AND PORE VOLUME
ARE VERY SENSITIVE TO pH.
THIS REFLECTS THE REDUCTION IN THE
CONDENSATION RATE WITH DECREASING pH.
CHANGING n WITH ADDITIONS
OF 2 M HCl
CHANGING n
WITH EQUIVALENT
ADDITIONS OF H_2O
REFRACTIVE INDEX, n
V_p PORE VOLUME (%)
pH
1.39
1.37
1.35
1.33
1.31
1.29
1.27
1.25
1.24
5.76
10.34
14.99
19.70
24.48
29.31
34.21
1
2
3
4

Coating Rate Dependence of n